Spectral fiber sensors for cancer diagnostics *in vitro*

V. Artyushenko[a], F. Schulte[a], U. Zabarylo[a], H.-P. Berlien[b], I. Usenov[a, c],
T. Saeb Gilani[a, c], H. Eichler[c], Ł. Pieszczek[d], A. Bogomolov[e], H. Krause[f], O. Minet[g]

[a]art photonics GmbH, Rudower Chaussee 46, 12489 Berlin, Germany;
[b]Lasermedizin-Evangelische Elisabeth Klinik, Lützowstraße 24-26, 10785 Berlin, Germany;
[c]Technical University of Berlin, Institute for Optics & Atomic Physics, Straße des 17. Juni 135, 10623 Berlin, Germany;
[d]University of Silesia, Institute of Chemistry, Bankowa 14, 40-007 Katowice, Poland;
[e]Samara State Technical University, Molodogvardeyskaya 244, 443100 Samara, Russia,
[f]Charité Universitätsmedizin Berlin, Dept. of Urology, Charitéplatz 1, 10117 Berlin, Germany;
[g]Charité Universitätsmedizin Berlin, Medical Physics and Optical Diagnosis, Fabeckstraße 60-62, 14195 Berlin, Germany

ABSTRACT

Cancer is one of the leading causes for morbidity and mortality worldwide. Therefore, efforts are concentrated on cancer detection in an early stage to enhance survival rates for cancer patients. A certain intraoperative navigation in the tumor border zone is also an essential task to lower the mortality rate after surgical treatment. Molecular spectroscopy methods proved to be powerful tools to differentiate cancerous and healthy tissue. Within our project comparison of different vibration spectroscopy methods were tested to select the better one or to reach synergy from their combination.

One key aspect was in special fiber probe development for each technique. Using fiber optic probes in Raman, MIR and NIR spectroscopy is a very powerful method for non-invasive in vivo applications. Miniaturization of Raman probes was achieved by deposition of dielectric filters directly onto the silica fiber end surfaces. Raman, NIR and MIR spectroscopy were used to analyze samples from kidney tumors. The differentiation between cancer and healthy samples was successfully obtained by multivariate data analysis.

Keywords: cancer diagnostics, MIR spectroscopy, NIR spectroscopy, Raman spectroscopy, fiber optic probe

1. INTRODUCTION

According to the world cancer report in 2014[1] cancer is one of the leading causes for morbidity and mortality worldwide. Around 14 million new cases and 8.2 million cancer related deaths were registered in 2012, and the number of new cancer patients diagnosed each year will rise by 20% between 2002 and 2020. Reports in the literature show[2] that up to 30% of surgical procedures result in an incomplete removal of the tumor. The task to define tumor margins in-vivo is a great challenge, and optical spectroscopy may solve this problem.

Malignant and healthy tissue may be differentiated by fluorescence or molecular spectroscopy methods - like Raman scattering, IR-absorption or diffuse reflection. Raman spectroscopy has already been successfully applied to detect skin cancer[3]. Also the performance power of MIR[4], NIR[5] and fluorescence[6] spectroscopy to detect cervical and breast cancer respectively was proven before.

However, the transference of these results into the hospital environment so far has not been successful. Reasons for that are high costs for the instruments and special training needed for the operators. Hence, easy to handle cheap instruments are needed. Moreover, the specificity and sensitivity of the results should outperform conventionally used methods. This goal could be accomplished through the combination of methods. Multi modal approaches for cancer detection are already being persuaded for example by Tunnell et al.[7]. However, the combination of Raman and MIR spectroscopy into one single instrument is new and very promising as those are complimentary methods.

After meticulous testing and comparison of different spectroscopic methods used for the same cancer samples the better technique or a combination of them can be found to design an optimal setup. The best method or their combination can be

*sa@artphotonics.com; phone +49 30 677 988 70; fax +49 30 677 988 799; artphotonics.com

derived from the best combination of key parameters: sensitivity, specificity and accuracy. First results are presented here for the differentiation of tissue removed from normal and tumorous parts of kidney.

Looking for future clinical applications all systems or sensors must be combined with flexible and tiny fiber probes – to be disposable or sterilizable. That way, the probes can be incorporated into endoscopes enabling free access to almost all body sites[8]. The Raman probes, developed within this project, use dielectric filters directly deposited onto the silica fiber end faces. This enables miniaturization of the fiber-optic probe head, reduces price of the instrument and allows the combination of all mentioned spectroscopic techniques in one probe without sacrificing signal-to-noise ratio and dimensions of the sensor. The quality of the dielectric coatings is crucial and determines the sensitivity of the probe.

2. MATERIALS & METHODS

Sample preparation

Matched pairs of tumor and adjacent nontumor renal cortex tissue were obtained from kidneys of patients who underwent radical nephrectomy in the Klinik für Urologie, Charité – Universitätsmedizin Berlin from November 2014 to February 2015. Histological classification was performed according to the WHO criteria. All patients gave their informed consent for this procedure in accordance with rules of the institutional ethics board (EA1/134/12).

To minimize data tampering by blood cells, all kidneys were perfused for 20min by ice-cold saline buffer immediately after nephrectomy. Afterwards tissue sections were obtained by a dedicated uropathologist, the extracted samples were snap-frozen immediately in liquid nitrogen and then stored in a freezer at -80°C in 1,5ml cryo-tubes in order to avoid autolytic decomposition processes. For the spectroscopic measurements snap-frozen samples from 3 different patients were selected from the Biospecimens Resources of Klinik für Urologie, Charité – Universitätsmedizin Berlin. All tumor blocks were reviewed by the pathologist and classified according to the Fuhrman nuclear grading system (FNG) predominantly as moderate or high grade (nuclear grades 2 and 3)[9]. The Fuhrman system of renal cell carcinoma consists of four grades based on features of nuclear size, nuclear shape and nucleolar prominence and is currently the most widely used grading protocol in Europe and North America. According to the FNG, grade 2 means slightly irregular contours and diameters of approximately 15µm with nucleoli visible at 400x and grade 3 – moderately to markedly irregular nuclear contours and diameters of approximately 20µm with large nucleoli visible at 100x.

The sample (M_178) was classified as chromophobe renal cell carcinoma (chRCC) and two other samples (M_179 and M_185) were clear cell renal cell carcinoma (ccRCC). The respective tumor formula was for patient M_178 – pT2bG2R0L0V1, for patient M_179 – pT3aG2R0L0V0, and for patient M_185 – pT3aG3R2L1V1, respectively. Clear cell renal cell carcinoma is the most prominent RCC subtype and potentially a highly vascularized and aggressive tumor.

Tumors were staged according to the Union for International Cancer Control Tumor-Node-Metastasis (UICC TNM)[10, 11] stage classification as follows: pT2b - Tumor more than 5cm in greatest dimension, extends into major veins or invades adrenal glands or perinephric tissue but not beyond Gerota's fascia stage and pT3a- tumor extension through renal capsule into perinephric or perisinuous fat or adrenal, but not beyond Gerota's fascia[12]. Treatment for RCC was in all cases radical nephrectomy (via laparoscopy, for tumor of grade 2) and via open surgery for tumor of grade 3. All biopsies were taken from the upper pole of the left kidney of female patients between 37 and 74 years of age.

Prior to measurement of the frozen biopsies, the specimens were thawed in tissue floating bath (C&A Scientific, Virginia, USA) at 37°C for 10-15 minutes and warmed up until they reached room temperature. Each measurement was conducted at room temperature (22-25°C). To prevent drying of tissue, samples were moisturized with warmed physiological saline solution (NaCl 0.9%).

Each tissue sample was about 10x15mm in size. For every patient a large petri dish of 94mm diameter with 2 smaller petri dishes of 35mm diameter were prepared. Tumor and normal biopsies were placed into each of the small petri dishes and labeled accordingly. In this way prepared samples were then successively measured by 3 spectroscopic methods.

IR

Infrared measurements have been performed using FTIR spectrometers Matrix-MF with MCT detector (Bruker, USA) and the iS5 with DTGS detector (Thermo Fisher Scientific, USA). Attenuated Total Reflection spectra (ATR) have been measured using two different ATR fiber optic probes. The probe based on Chalcogenide Infrared (CIR) fibers with

Zirconium dioxide ATR tip (art photonics GmbH, Germany) was used to obtain spectra in the range 2000-5000cm^{-1}. Spectra in the fingerprint region 600-1800cm^{-1} were recorded with Mid Infrared ATR probe with Polycrystalline Infrared (PIR) fibers and silicium ATR tip (art photonics GmbH, Berlin, Germany). Experimental parameters were set to 64 scans and resolution 8cm^{-1}. The resulting measurement times were about 1 and 3 minutes for Matrix MF and iS5 spectrometers, respectively.

Raman

All Raman experiments were performed using Ventana spectrometer (Ocean Optics, USA) coupled to fiber optic probes. For the spectra obtained in high wavenumber range (2500-4000cm^{-1}) a single fiber was used as both excitation and detection channel, simultaneously. The laser with 690nm wavelength (CNI Optoelectronics Technology, China) was coupled into the fiber (400μm core diameter, 0.5m length, art photonics GmbH, Germany) using a special coupler allowing delivery of laser radiation to the sample and back to the spectrometer via the same fiber. Measurements in the fingerprint region (600-1800cm^{-1}) were recorded with 785nm laser for excitation (Ocean Optics, USA) and a general purpose Raman probe (Ocean Optics, USA).

Ventana-785-Raman model was used with 50μm slit providing 10 cm^{-1} @ 810nm (FWHM) optical resolution. All Raman spectra of tissues were acquired with SpectraSuite spectroscopy software averaging 3 scans, with boxcar smoothing set to 3, integration time varied from 300 to 1000ms. Each sample was measured 10 times and spectra obtained with fiber probes in the air (without sample) were used to subtract the background caused by a setup.

NIR

The NIR measurements were done using the portable fiber optic NIR-Quest InGaAs spectrometer (Ocean Optics, USA) operating in reflectance mode in the spectral range 900-1700nm. The spectrometer was connected with the light source and the probe through optical fibers. Tungsten Halogen lamp (Ocean Optics, USA) was used as a light source.

The NIRQuest-512 model has a 25μm slit providing 3,1nm (FWHM) optical resolution. All reflectance spectra of tissues were acquired in Spectra Suite spectroscopy software averaging 5 scans, with boxcar smoothing set to 5. Each sample was measured 10 times with saline solution as a reference standard.

To ensure the reproducibility of measurements, the NIR-probe (7 collecting + 1 emitting 400μm fibers) was fixed on the adjustable table stand. An additional spacing cap on the probe tip provides the exact distance between tissue surface and probe during measurements.
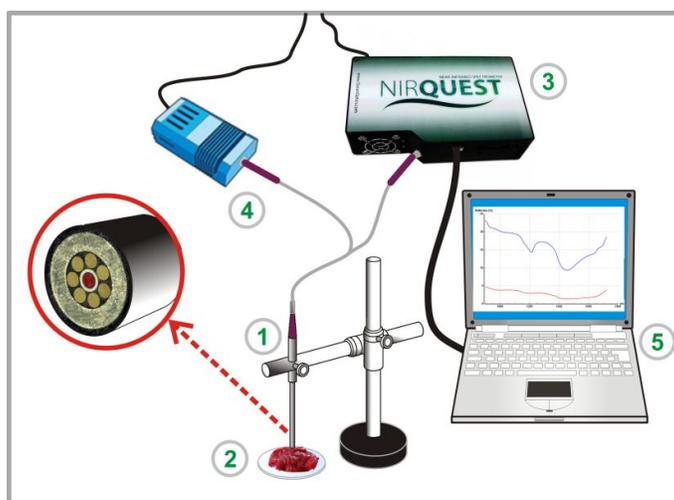

Figure 1. Setup for NIR measurements. (1)-NIR probe R(1+7) from art photonics GmbH [13], (2)-Tissue slice in petri dish, (3) NIRQuest spectrometer, (4)- halogen lamp, (5)- PC with software for spectra collection

Data analysis

Data analysis was performed in PLS Toolbox v7.5.2 (Eigenvector Research Inc., Manson, WA, USA) working under MATLAB R2008b (The MathWorks™ Inc., Natick, MA, USA).

Prior to further analysis all IR spectra were preprocessed using Standard Normal Variate (SNV) correction[14]. SNV alignment usually results in better prediction power and decreases the complexity of chemometric models. The aim of SNV is to remove scattering, spectral noise and other systematic variations of the baseline. The transformation normalizes spectra to the unit vector length and is achieved by dividing mean-centered spectra by the standard deviation.

In the case of NIR measurements first of all the linear baseline effects were eliminated by taking of first derivative with Savitzky-Golay[15] algorithm (nine point moving window width and polynomial of degree two). To reduce spectral differences due to the tissue thickness and scattering effects, we used further SNV normalization.

For an exploratory unsupervised qualitative analysis of spectral data the Principal Component Analysis (PCA) was used. PCA performs a bilinear decomposition of a source data matrix $\mathbf{X}$ ($n \times m$, n samples in rows and m variables in columns) into two complementary matrices: scores $\mathbf{T}$ ($n \times a$) and loadings $\mathbf{P}$ ($m \times a$):

$$\mathbf{X} = \mathbf{TP}^{\mathrm{T}} + \mathbf{E} = \sum_{i=1}^{a} \mathrm{t}_i \mathrm{p}_i^{\mathrm{T}} + \mathbf{E}, \tag{1}$$

where $a << n,m$ is the number of principle components (PCs); t_i ($n \times 1$) and p_i ($m \times 1$) are the orthogonal/orthonormal vectors constituting the matrices $\mathbf{T}$ and $\mathbf{P}$, respectively. The matrix product of $\mathbf{T}$ and $\mathbf{P}^{\mathrm{T}}$ reproduces the most important variance in $\mathbf{X}$, leaving the irrelevant information (error) in a residual matrix $\mathbf{E}$ ($n \times m$). Therefore, PCA is an X-data projection onto a-dimensional PC space, where it can be effectively presented and analyzed. The method is particularly advantageous for the analysis of spectroscopic data with a large number of mutually correlated variables.

The matrices $\mathbf{T}$ and $\mathbf{P}$ provide useful information about the data internal structure. Their interpretation is based on the fact that similarity of two objects (samples) corresponds to the distance between them in the PC-space. Pair-wise $\mathrm{t}_i - \mathrm{t}_j$ score plots, in particular, $\mathrm{t}_1 - \mathrm{t}_2$ are often referred to as 'object maps'. They are commonly used to reveal sample groups or classes and discriminate between them. Similarly, the loading plots ('variable maps') show the variable correlations. The distance from the origin of the score plot to the sample reflects its importance for the model. In the present work PCA scores were used to investigate the classes of healthy and malignant tissues.

3. RESULTS & DISCUSSION

MIR spectra recorded from cancer and non-cancer tissues show contributions from lipids, proteins and carbohydrates. Averaged spectra obtained from kidney samples of three patients are shown in figure 2. Signal intensities are comparable in the range from 1300cm^{-1} up to 1800cm^{-1}. The absorption peaks at 1740, 1460 and 1378cm^{-1} can be assigned to lipids. They are due to C=O stretching, CH$_3$ asymmetric and CH$_3$ symmetric bending vibrations, respectively. The Amide bands can be seen at 1650, 1560 and 1300cm^{-1}. In the range up to 1250cm^{-1} distinct variation can be observed. Typical bands caused by phosphate group of phospholipids can be found at 1085 and 1240cm^{-1}. So called phosphate group is referring to the phosphor-diester-linkage present in phospholipids. However, this group can also be found in DNA and RNA. Furthermore, polysaccharides and collagen contribute to characteristic signals within this wavenumber range. The prominent band around 1040cm^{-1} is most likely due to sugar molecules which can also be found in DNA (Tentative peak assignments were made in accordance with literature[16,17]).

Based on these assignments it is difficult to decide which chemical group is responsible for the clear spectral differences observed between non-cancer and cancer tissue as most signals are overlapping. Different spectral markers typical for cancer signals were published before. For example, Tobin et al.[18] found that the intensity of Amide I band is increased in cancer tissue. Our results are showing the opposite trend, this clarifies that further investigations are essential for the understanding of cancer spectra.
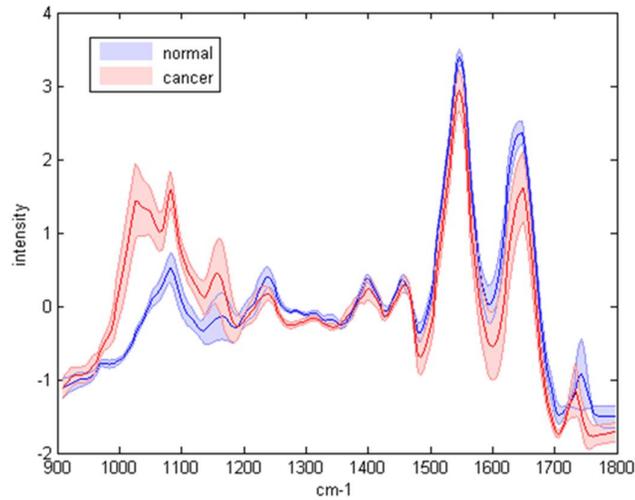
Figure 2. MIR spectra obtained from two patients, samples were generated from healthy and cancerous tissue. Here, the average spectra with standard deviation are depicted.

In figure 2 only MIR spectra from two patients (178, 179) are shown. Three tumor samples showed striking differences in their MIR spectra as well as in their physical appearance. The specimens 178 and 179 show a so called colliquation necrosis due to excessive tumor growth in contrast to the more fibrous tumor structure of patient 185. That is why sample 185 is excluded from this view.

The results of PCA can be seen in figures 3 and 4. For figure 3 spectra from all three patients were used, a separation for cancer and normal samples could not be achieved. In the PCA-model based on MIR-spectra there is some overlap between healthy and cancer samples related to the nature of the sample 185 as discussed before. For further evaluation this sample was excluded. In the resulting projection (shown in figure 4) cancer spectra and spectra belonging to the healthy set of samples are lying in different areas in the multivariate space. The exploration which was performed using PCA shows that there is a difference between cancer and normal tissue, especially in the range from 950 to 1200cm^{-1}. Although in the future, a bigger set of samples should be measured to indicate definitely that there is general difference between cancer and healthy tissues as to the ratio of the main components.
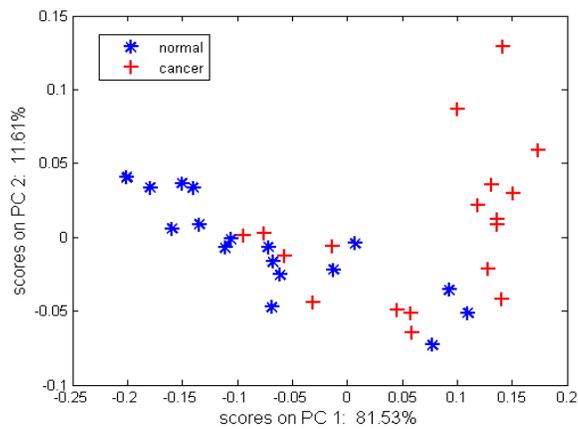

Figure 3. PCA projection of MIR spectra obtained from three patients (samples were taken from normal and cancer tissue).
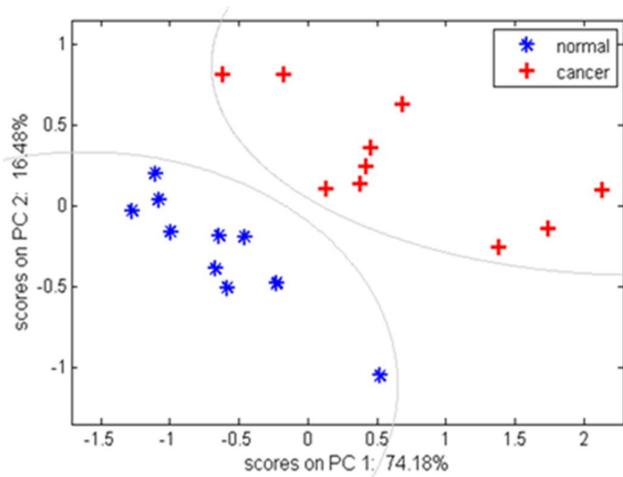
Figure 4. PCA projection of MIR spectra obtained from two patients (samples were taken from normal and cancer tissue)

MIR spectra discussed so far were recorded in the fingerprint region from 900 to 1800cm^{-1}. The signals detected in this part of the spectrum are derived from C=C and C=O stretching vibrations as well as from bending and skeletal vibrations. Whereas NIR measurements are performed from 13000 to 4000cm^{-1} – with bands originated from overtones and combinations of C-H, N-H and O-H stretching vibrations. This spectral range enables to detect cancerous samples.
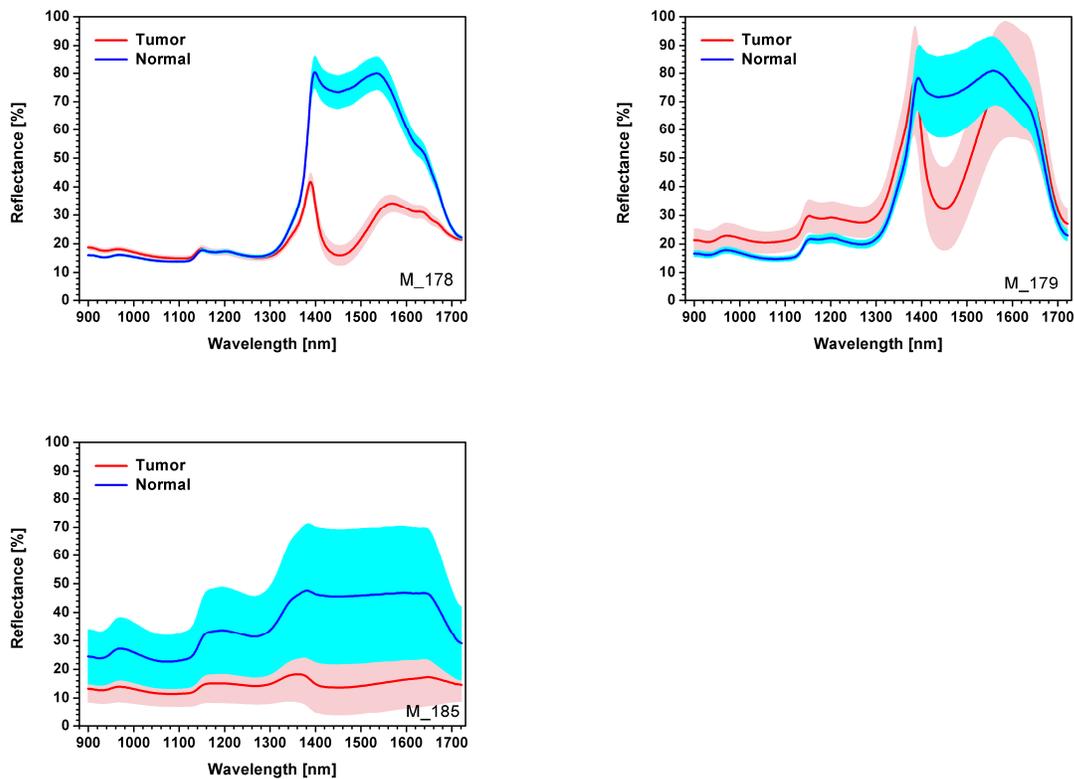

Figure 5. Mean ± standard deviation spectra of cancer and normal tissue obtained from NIR-measurements of three patients.

The relatively high variation between three patients could be due to the different stages of carcinogenesis. Additionally, the differences in thickness and consistency of the samples are affecting the spectral reflectance due to varying penetration depths of photons. NIR spectra include much information on chemical composition of the tissue and its alteration, this can be used for diagnostic purposes as well. NIR spectrum is a composition of different spectral signatures of components like lipids, proteins, carbohydrates and phosphate. There are specific spectral regions, which show higher variation of composition between normal and tumor tissue. To highlight them, we used mathematical preprocessing. The aim of signal pretreatment is to improve data quality before modeling and remove physical information from the spectra which can be significantly influenced by nonlinearities introduced by light scattering. Applying a pretreatment can increase the repeatability/reproducibility of the method, model robustness and accuracy.

Differences between cancer and normal spectra were emphasized by subtracting the cancer mean spectrum from the normal mean spectrum. This was done for every patient.

Figure 6 depicts SNV normalized mean spectra including standard deviation obtained from the first derivatives of the spectra from cancerous and normal kidney tissue. The lower part of this figure shows the difference spectra. Also provided in Figure 6 are the assignments of bands to different chemical substructures. There are three characteristic regions corresponding to NH and CH combinations, CH second overtones and first overtones of OH, NH, and CH combination vibrations, respectively.
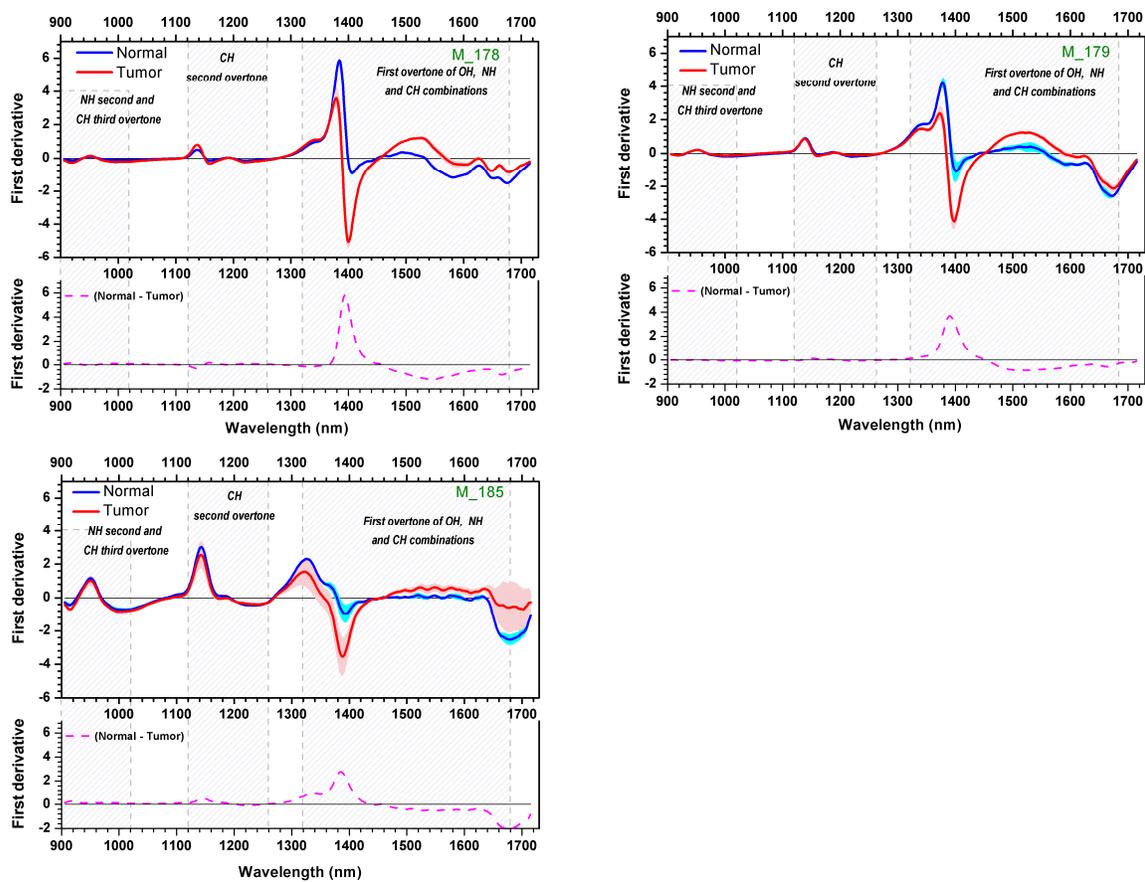

Figure 6. Preprocessed spectra showing clear differences between cancerous and non-cancer samples.

The biggest spectral differences between cancer and normal tissues were observed in the interval characteristic for first overtones and combination vibrations of OH, NH and CH bonds. It is well known that carbohydrate level is reduced in cancer tissues as compared to the normal tissue and phosphate content of normal tissues is higher than cancerous ones[19]. Our results indicate that the first and the second overtones of C-H vibrations as well as the combination bands of OH, NH and CH can serve as diagnostic markers for kidney cancer. Like with many other tumors[20] the CH vibration regions seem to be crucial determinants to distinguish between normal tissue and renal tumor.

With the help of multivariate analysis the differences already observable with preprocessed spectra can be further emphasized. Two classes are successfully separated as can be seen below (figure 7). Preprocessing by Savitzky-Golay 1st derivative (2nd order polynomial, window width of 15 points) followed by SNV correction prior to PCA analysis provides both sample type (Normal or Tumor) and patient separation.
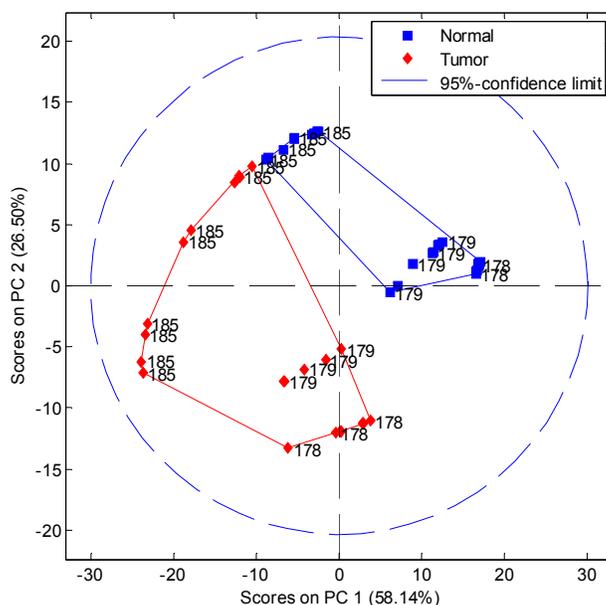

Figure 7. PCA scores for NIR spectra from three patients.

Also the differentiation between cancer and non-cancer samples seemed to be very straight forward based on Raman spectroscopy. Cancer samples did not display fluorescence whereas the non-cancer samples showed very strong fluorescence that covered almost all Raman signals. At the moment, the reason for this fluorescence is unknown (it is to be investigated in following experiments). Therefore no multivariate analysis was performed for the Raman spectra as the fluorescence would falsify the results.

Nonetheless, one exemplary spectrum obtained from kidney cancer can be seen in figure 8. The signals in the lower wavenumber range show low intensities. Typical signals found in this range are due to skeletal vibrations of amino acids. For example, the C-S stretching mode of cysteine is found around $660 cm^{-1}$. Raman bands showing higher intensities are situated at 1300, 1441 and $1660 cm^{-1}$. Those vibrations can be assigned to CH_2CH_3 twisting, CH_2 bending and C=O stretching modes, respectively. The first signal is derived from lipids or collagen, whereas the last signal is caused by proteins and the remaining signal can be generated by both biomolecules. As the band at $1520 cm^{-1}$ can be clearly assigned to carotenoids it is deducted that the signals close to 1000 and $1150 cm^{-1}$ are also derived from this molecule. About 600 different carotenoids are known within nature and all are based upon the structure of isoprene. Actually, the position and shape of the C=C stretching vibration at $1520 cm^{-1}$ can be used to elucidate how many double bonds the carotenoids present in the sample possess[21]. However, the quality of our spectra would need to be enhanced for this evaluation.
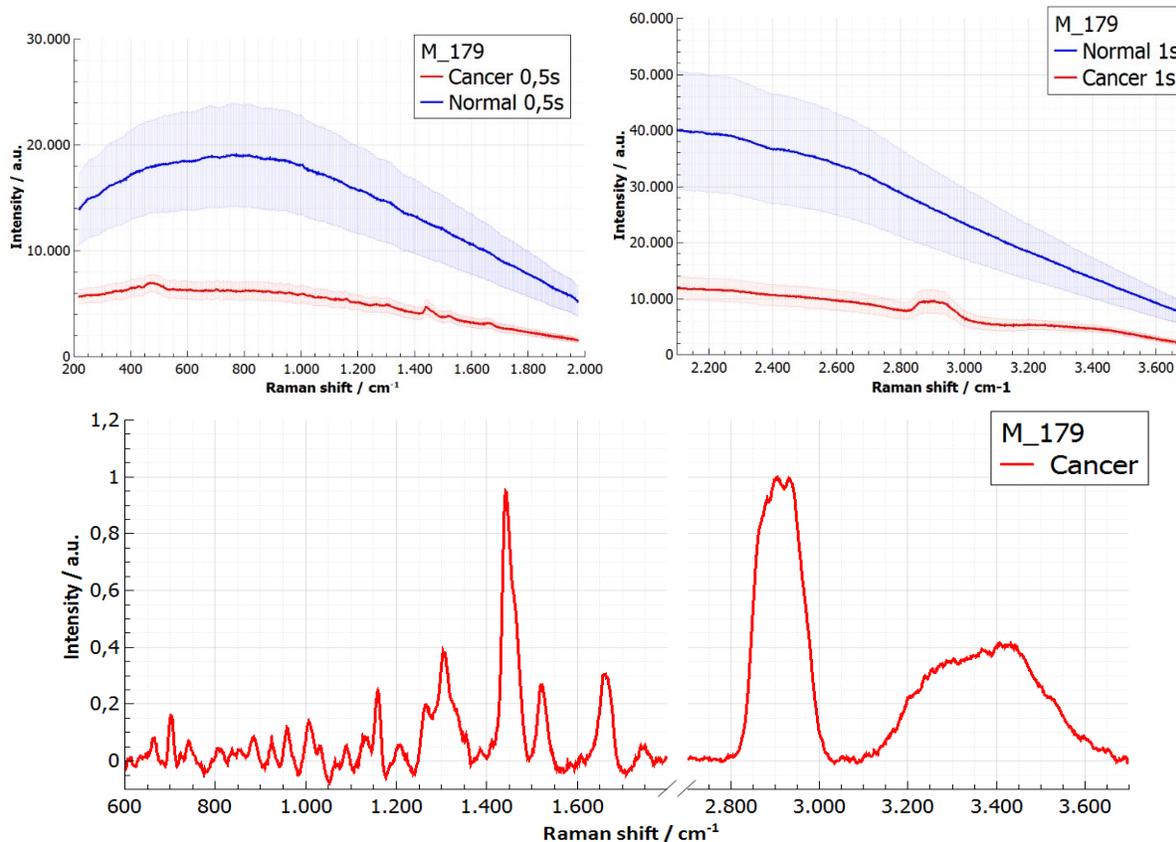
Figure 8. Raman spectra obtained for patient M-179 are shown above – with a clear differences between cancer and healthy parts of kidney in fingerprint range (left) and in high wavenumber region (right). Raman spectra for these ranges are shown in the bottom for cancer tissue only after fluorescence background subtraction – as it was too weak for healthy tissue.

The Raman spectra in the high wavenumber region were excited with a 690nm laser. The same behavior as for the spectra obtained with 785nm was noticed; the fluorescence was higher for the non-cancer samples as for the cancer samples. Within this region certain signals can be assigned to vibrational modes of lipids, proteins and water. Lipids show distinct peaks at 2920 and 2850cm^{-1}corresponding to the anti-symmetric and symmetric CH_2 stretching vibrations. Proteins cause peaks at 2956 and 2870cm^{-1} correlating to the stretching vibrations of the CH_3 group. The characteristic broad band for water is located at 3400cm^{-1}.

4. CONCLUSIONS

The preliminary work presented here proves that molecular spectroscopy can be used to differentiate between cancer /non-cancer tissue and that the investigated methods complement each other. This can be seen as a starting point towards the development of a multimodal instrument for the detection of cancer. On this way, we will have to switch from ex-vivo to in-vivo measurements as well as enhance our technical equipment - in particular the probes. Furthermore, higher numbers of samples have to be analyzed to strengthen our multivariate methods.

Acknowledgement

Investing in **your** future!

EUROPEAN UNION
European Regional
Development Fund
www.efre.brandenburg.de

REFERENCES

[1]   Stewart, B. and Wild C., [World Cancer Report], International Agency for Research on Cancer, (2014).

[2]   Bogdanov-Berezovsky, A. , Cohen, A.D, Glesinger, R., Cagnano, E., Rosenberg, L.¸ "Risk factors for incomplete excision of squamous cell carcinomas". J Dermatolog Treat., 16(5-6), 341-4 (2005).

[3]   Schleusener, J., Gluszczynska, P., Reble, C., Gersonde, I., Helfmann, J., Cappius, H., Fluhr, J., Meinke, M., „Perturbation Factors in the Clinical Handling of a Fiber-Coupled Raman Probe for Cutaneous In Vivo Diagnostic Raman Spectroscopy". Appl. Spectrosc., 69(2), 243-256 (2015).

[4]   Purandare, N., Patel, I., Trevisan, J., Bolger, N., Kelehan, R.; Bünau, G., Martin-Hirsch, P., Prendiville, W., Martin, F., „Biospectroscopy insights into the multi-stage process of cervical cancer development: probing for spectral biomarkers in cytology to distinguish grades", Analyst 138, 3909-3916 (2013).

[5]   Lisanne de Boer, EPIC Workshop in Rotterdam on July 2-3rd, 2014.

[6]   Gupta, P., Majumder, S., Uppal, A., "Breast cancer diagnosis using N_2 laser excited autofluorescence spectroscopy", Lasers in Surgery and Medicine 21(5), 417-422 (1997).

[7]   Sharma, M., Lim, L., Marple E., Riggs, W., Tunnell, J., "Development and Characterization of a Multi-Modal Probe for Early Skin Cancer Detection using Raman, Reflectance and Fluorescence Spectroscopies", Biomedical Optics and 3D Imaging (2012).

[8]   Latka, I., Dochow, S., Krafft, C., Dietzek, B., Popp, J., „Die faseroptischen Sonden für lineare und nichtlineare Raman-Anwendungen - Aktuelle Trends und zukünftige Entwicklung", Laser Photonics Rev 7(5), 698-731 (2013).

[9]   Fuhrman, S.A., Lasky, L.C., Limas, C., "Prognostic significance of morphologic parameters in renal cell carcinoma," Am J Surg Pathol. Oct;6(7):655-63 (1982).

[10]   AJCC (2002) Cancer staging manual, 6th edn. Springer, Berlin.

[11]   Sobin, L.H, Wittekind, C., "TNM Classification of Malignant Tumours" (6th edition).New York: Wiley-Liss; 2002.

[12]   Berufsverband Deutscher Pathologen. Anleitung zur pathologisch-anatomischen Diagnostik von Tumoren des Nierenparenchyms. 2009.

[13]   http://www.artphotonics.de/products/spectroscopy-fiber-probes-and-probe-couplers/fiber-probes-for-process-spectroscopy/

[14]   Barnes, R.J., Dhanoa, M.S., Lister S.J.: "Standard Normal Variate Transformation and De-trending of Near-Infrared Diffuse Reflectance Spectra", Appl. Spectrosc. 43, 772-777 (1989).

[15]   Savitzky, A., Golay, M. J. E.: "Smoothing and differentiation of data by simplified least squares procedures," Analytical Chemistry, vol. 36, no. 8, pp. 1627–1639, (1964).

[16]   Diem, M., Griffiths, P.R., Chalmers, J. M., [Vibrational Spectroscopy for Medical Diagnosis], Wiley, 43-45 (2008).

[17]   Stuart, B., [Infrared Spectroscopy: Fundamentals and Applications], Wiley, 71-92 (2004).

[18]   Tobin, M.J., Chesters, M.A., Chalmers, J.M., Rutten, F.J., Fisher, S.E., Symonds, I.M., Hitchcock, A., Allibone, R., Dias-Gunasekara, S., "Infrared microscopy of epithelial cancer cells in whole tissues and in tissue culture, using synchrotron radiation," Faraday Discuss., 126:27-39, (2004).

[19]   Chen, H., Lin, Z., Mo, L., Wu, T., & Tan, C., "Near-Infrared Spectroscopy as a Diagnostic Tool for Distinguishing between Normal and Malignant Colorectal Tissues", BioMed Research International, 472197 (2015).

[20]   Kondepati, V.R., Oszinda, T., Heise, H.M, et all, "CH-overtone regions as diagnostic markers for near-infrared spectroscopic diagnosis of primary cancers in human pancreas and colorectal tissue", Anal Bioanal Chem, Mar;387(5), 1633-41 (2015).

[21]   Veronelli, M., Zerbi, M., Stradi, R., "In situ resonance raman spectra of carotenoids in bird's feathers," J. Raman Spectrosc., 26: 683–692 (1995).